CHEMICAL SCIENCES AND TECHNOLOGY

Seed Money Fund

Carbonation of Serpentine for Long-Term CO_2 Sequestration

J. G. Blencoe,[1] L. M. Anovitz,[2] J. S. Beard,[3] and D. A. Palmer[1]
[1]*Chemical Sciences Division*
[2]*University of Tennessee, Knoxville*
[3]*Virginia Museum of Natural History*

Results of autoclave experiments show that serpentine [$Mg_3Si_2O_5(OH)_4$] can be quantitatively converted to magnesite ($MgCO_3$) + silica (SiO_2) + water in a multistep chemical process that is much more energy efficient than the "direct" method for achieving that conversion. In the new process, serpentine is reacted in a concentrated solution of caustic soda (NaOH), producing brucite [$Mg(OH)_2$] + solubilized silica. The brucite- and silica-rich liquid are then physically separated to allow (1) reaction of the liquid with CO_2 to form bicarbonate ion + silica gel + water and (2) reaction of the bicarbonate ion with the brucite formed previously to produce magnesite + aqueous NaOH + water. The number of moles of NaOH produced during magnesite crystallization is exactly equal to the number of moles of that base consumed during conversion of serpentine to brucite; therefore, there is no net consumption of NaOH in the process. In addition, because the process produces separate streams of high-purity silica and magnesite, both of these solids become valuable commercial by-products. Fully optimized for a reactor-based mineral-carbonation technology implemented at large point sources of CO_2, the new serpentine-carbonation process provides a safe and effective means for permanently sequestering huge masses of CO_2.

Introduction

Mineral carbonation is a promising technology for reducing CO_2 emissions from fossil fuel-fired power plants, cement factories, and steel mills.[1] It involves reacting CO_2 with non-carbonate (predominantly silicate) minerals to form one or more thermodynamically stable and environmentally benign carbonate compounds. The process mimics natural weathering of silicate minerals to form carbonate minerals such as calcite ($CaCO_3$), dolomite [$CaMg(CO_3)_2$], magnesite ($MgCO_3$), and siderite ($FeCO_3$). However, natural mineral carbonation reactions are very sluggish at ambient temperature and pressure; therefore, one of the principal technical challenges for CO_2 sequestration by mineral carbonation is to develop one or more commercially viable chemical processes that significantly accelerate the rates at which silicate minerals are transformed to stable, crystalline carbonates.[2] Physicochemical factors that affect mineral carbonation reaction rates (kinetics) include process temperature, pressure, CO_2 fugacity, and redox state; the mass proportions of the reactants, "additives," and catalysts; pretreatment and size reduction of the mineral feedstock; and the overall solution chemistry of the liquid phase. Several potential silicate feedstocks for industrial-scale mineral carbonation have been proposed and evaluated, with greatest attention being given to olivine (Mg_2SiO_4) and serpentine [$Mg_3Si_2O_5(OH)_4$].[3–5] The carbonate produced by olivine/serpentine carbonation, magnesite, is highly stable and environmentally neutral in nearly all terrestrial environments.

An early olivine/serpentine carbonation scheme involved production of magnesite by (1) acid (HCl) decomposition of olivine ± serpentine, producing brucite [$Mg(OH)_2$] + silica (SiO_2) and (2) reaction of the $Mg(OH)_2$ with CO_2 to form magnesite.[1,3] However, a detailed feasibility study of this approach has shown that it is too energy intensive for industrial-scale implementation.[2] Therefore, over the past five years, attention has been focused on CO_2 sequestration by "direct" carbonation of olivine and serpentine.[6,7] In this method, CO_2 is sequestered in magnesite with no acid pretreatment of the silicate feedstock, and the primary reactants are olivine and/or serpentine, and supercritical CO_2. For olivine, the overall reaction is

$$Mg_2SiO_4 + 2CO_2 \rightarrow 2MgCO_3 + SiO_2 \ ; \qquad (1)$$

the corresponding reaction for serpentine is

$$Mg_3Si_2O_5(OH)_4 + 3CO_2 \rightarrow 3MgCO_3 + 2SiO_2 + 2H_2O \ . \qquad (2)$$

Recent experiments performed to determine the kinetics of these reactions indicate that, at a given elevated temperature and pressure—and using essentially identical kinds and amounts of "additives" and catalysts ($NaHCO_3$ and NaCl)—olivine reacts with CO_2 much more readily than serpentine.[6] This is unfortunate because, while

significant masses of olivine-bearing rocks exist for sequestering CO_2, naturally occurring serpentine is approximately an order of magnitude more abundant.[4,5] To date, the only remedy for sluggish serpentine reaction is to heat it to 600–650°C prior to carbonation, which drives off structurally bound water (hydroxyl groups).[6] Tests of this altered (dehydroxylated) serpentine have shown that it is much more reactive than untreated (hydroxylated) serpentine. However, at a typical fossil fuel–fired power plant, heat treating serpentine at 600–650°C prior to carbonation would require ~200 kW·h of electricity per ton of serpentine feedstock.[6] With 1 ton of carbon in a fossil fuel producing ~3.7 tons of CO_2, and each ton of CO_2 consuming ~2 tons of serpentine during carbonation, the power requirements for serpentine dehydroxylation represent 20–30% of total power output. This large energy penalty threatens the economic viability of CO_2 sequestration by serpentine carbonation.

Technical Approach

In this study, olivine/serpentine carbonation was investigated at elevated temperatures and pressures using conventional methods of hydrothermal experimentation. Solid, liquid, and gaseous reactants were the following: finely ground natural serpentine (antigorite variety from the Cedar Hill Quarry, Lancaster County, PA) and olivine (from Twin Sisters Peak, Washington), fine-grained brucite formed by caustic decomposition of the natural serpentine, reagent-grade synthetic sodium silicate (Na_2SiO_3), a 50 wt % solution of caustic soda, and research-grade (99.999% pure) CO_2 dispensed from a standard gas cylinder fitted with a dip-tube. These starting materials were loaded into a 1.75-inch O.D., 1.40-inch I.D., 6.28-inch long, closed-one-end Teflon liner; inserted into a 300-mL, bolted-closure autoclave (Fig. 1); heated to experimental temperature in an AC-powered resistance furnace; and allowed to react for periods ranging from 2 h to 3 days. Experimental temperatures were 22 and 200°C, and experimental pressures ranged from ~10 to 64 atm. Experiments were concluded by switching off furnace power, allowing the autoclave to cool to a temperature below ~40°C, and when necessary, venting any high-pressure CO_2 that remained in the autoclave. [Note: numerous experiments were conducted with no high-pressure CO_2 in the autoclave.] After each experiment, reacted solids were removed from the autoclave, dried in a forced-air convection oven, and examined by optical microscopy, scanning electron microscopy (SEM, Fig. 2), powder X-ray diffractometry, and/or electron-probe microanalysis. Phase identification was sufficient to achieve the main aims of the project; therefore, no attempts were made to determine the minor- or trace-element contents of the reacted solids, or the relative proportions of solid products (when more than one solid compound was formed during an experiment).

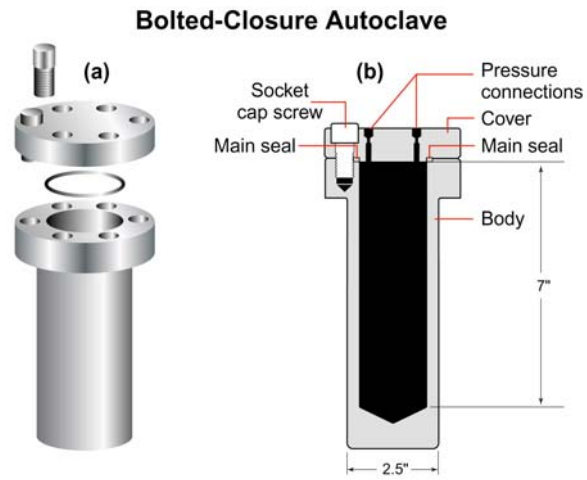

Fig. 1. Schematic illustrations of the bolted-closure autoclave used to perform hydrothermal experiments in this study: (a) perspective view, and (b) cross section through the middle of the vessel.

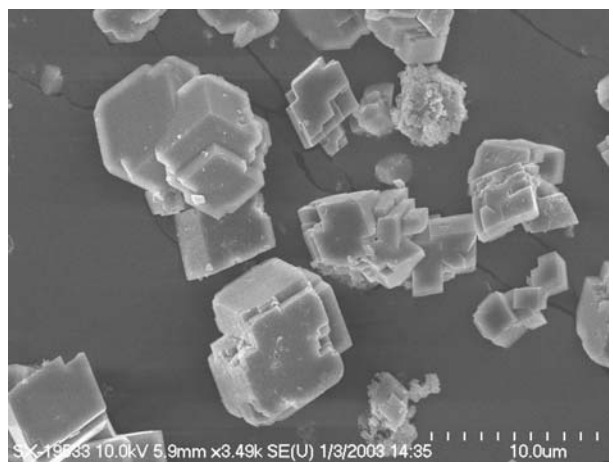

Fig. 2. Secondary electron SEM image of magnesite crystals grown by reacting brucite with CO_2 (Reactions 6 and 11).

Results and Accomplishments

The principal goal of the research was to develop a serpentine-carbonation process that is energetically superior to the direct method discussed above (Reaction 2). To achieve that objective, more than 40 autoclave experiments were performed. The resulting phase equilibrium data are definitive, collectively indicating that hydroxylated serpentine is converted to magnesite most efficiently by the following multistep process.[8] First, the serpentine feedstock is reacted with a concentrated solution of caustic soda (NaOH) to produce crystalline brucite and an aqueous fluid rich in dissolved silica. Written in ionic form, the reaction is

$$Mg_3Si_2O_5(OH)_4 + 2OH^- + 3H_2O \rightarrow 3Mg(OH)_2(\downarrow) + 2\ SiO(OH)_3^- \ . \quad (3)$$

[Note: Na^+ ions present in the caustic solution do not participate in serpentine → brucite conversion. Therefore, they have been omitted from Reaction 3.] Next, the solid and liquid products of caustic treatment are physically segregated for the second and third steps of the process, which are, respectively, (i) decomposition of $SiO(OH)_3^-$ by the reaction

$$2\ SiO(OH)_3^- + 2CO_2(aq) \rightarrow 2HCO_3^- + 2SiO_2(\downarrow) + 2H_2O \quad (4)$$

and (ii) carbonation of brucite by the reactions

$$2Mg(OH)_2 + 2HCO_3^- \rightarrow 2MgCO_3(\downarrow) + 2OH^- + 2H_2O \quad (5)$$

and

$$Mg(OH)_2 + CO_2 \rightarrow MgCO_3 + H_2O \ , \quad (6)$$

where the HCO_3^- used to carbonate brucite in Reaction 5 is formed in step 2 of the process (Reaction 4). The OH^- "regenerated" in Reaction 5 is then used to convert more serpentine to brucite (Reaction 3). Reactions 3–6 form the basis for a mineral carbonation technology that produces magnesite by the *net* reaction

$$Mg_3Si_2O_5(OH)_4 + 3CO_2 \rightarrow 3MgCO_3 + 2SiO_2 + 2H_2O \ , \quad (7)$$

which is identical to the direct serpentine-carbonation reaction discussed above (Reaction 2). Significantly, our experimental data also indicate that olivine is converted to magnesite by a multistep process that is very similar to the one developed for carbonation of serpentine (Reactions 3–6): viz.,

$$Mg_2SiO_4 + OH^- + 3H_2O \rightarrow 2Mg(OH)_2(\downarrow) + SiO(OH)_3^- \ , \quad (8)$$

$$SiO(OH)_3^- + CO_2(aq) \rightarrow HCO_3^- + SiO_2(\downarrow) + H_2O \ , \quad (9)$$

$$Mg(OH)_2 + HCO_3^- \rightarrow MgCO_3(\downarrow) + OH^- + H_2O \quad (10)$$

and

$$Mg(OH)_2 + CO_2 \rightarrow MgCO_3 + H_2O \ . \quad (11)$$

Adding up Reactions 8–11 yields the net reaction

$$Mg_2SiO_4 + 2CO_2 \rightarrow 2MgCO_3 + SiO_2 \ , \quad (12)$$

which is identical to the direct olivine-carbonation reaction discussed previously (Reaction 1).

Considering that the solid phases and proportions of solids produced by the multistep carbonation method (Reactions 3–6 and 8–11) and the direct method (Reactions 1 and 2) are identical, it could be concluded that the two approaches are nothing more than different chemical pathways to the same overall result. However, several aspects of the multistep method give it important advantages over the direct method. First, because both olivine and (hydroxylated) serpentine are rapidly decomposed by caustic soda at very low temperatures (≤200°C) in the multistep method, no special pretreatment of the silicate feedstock is required. This contrasts sharply with the direct method for serpentine carbonation, which requires extreme grinding and/or high-temperature (600–650°C) heat pretreatment of the feedstock to ensure satisfactory reactivity.[6] Second, in the multistep method, the fluid pressure required to achieve rapid and efficient carbonation is <10% of that applied in the direct method (i.e., ~15 atm in the multistep method versus 185 atm in the direct method). Therefore, future mineral-carbonation reactors that implement the multistep method at the power-plant scale would require no expensive pressure-intensifying equipment. Third, in the multistep method, separate streams of silica gel and magnesite are produced, allowing each (nearly pure) substance to be used as a raw material for various commercial applications. In contrast, the direct method generates a single stream of solid material, consisting of intimately mixed silica gel and magnesite. The high costs of separating these materials effectively precludes any value-added commercial utility of the solid effluent. In addition, because gelatinous silica is readily mobilized by meteoric water, it is an inherently undesirable waste product for near-surface disposal. Thus, compared to separate masses of its individual components, mixtures of silica gel and magnesite are an economic liability.

The relative merits of the direct and multistep methods for olivine/serpentine carbonation could be assessed more fully by quantitatively comparing their overall kinetics and energetics; determining the capital and operating costs of the different kinds of reactors and processing protocols that would be required to implement each method in industrial settings; accurately calculating the costs of dealing with large masses of mixed silica and magnesite; and completing a detailed cost/benefit analysis of using silica gel and magnesite to create commercially viable byproducts. Unfortunately, these assessments are very difficult to perform at the present time due to a lack of detailed technical and economic information on the particular manner in which each carbonation method would be applied in reducing CO_2 emissions generated by industrial activity.

Summary and Conclusions

Multistep olivine/serpentine carbonation processes have been developed for sequestering CO_2 in industrial settings. The new method has the great advantage that it

avoids the following serious technical problems associated with the "direct" method for olivine/serpentine carbonation, viz., the need to dehydroxylate serpentine prior to carbonation, the necessity of pressurizing CO_2 to ~185 atm to achieve carbonation by reaction with supercritical CO_2, and production of a single solid effluent consisting of intimately mixed silica gel and magnesite. These problems are avoided in the new process by using caustic soda, rather than supercritical CO_2, as the rock "solvent," and by completely converting gaseous CO_2 to aqueous bicarbonate ion prior to forming magnesite. The main challenges for olivine/serpentine carbonation by the multistep method arise in separating reaction products formed in the first three steps of each process. Specifically, the multistep method relies on efficient and cost-effective separations of residual OH^- from $SiO(OH)_3^-$ in step 1 (Reactions 3 and 8), HCO_3^- from silica gel in step 2 (Reactions 4 and 9), and OH^- from residual HCO_3^- in step 3 (Reactions 5 and 10). Potential processing procedures for achieving these separations include the following: in step 1, precipitating solid NaOH by boiling off water; in step 2, gently centrifuging the aqueous solution to physically segregate the silica gel from the HCO_3^--rich aqueous fluid; and in step 3, adding "excess" $Mg(OH)_2$ (produced in step 1) to the reactants to ensure maximum consumption of bicarbonate ion during magnesite precipitation. [Note: In both olivine and serpentine carbonation by the multistep method, the solid effluents of step 3 (magnesite + residual brucite) are reacted with CO_2 in a fourth and final processing step to achieve the maximum possible production of magnesite (Reactions 6 and 11).]

By further demonstrating that olivine/serpentine carbonation is a potentially viable option for sequestering large masses of CO_2 produced by combustion of fossil fuels, the results of this study benefit governmental departments and agencies in both the United States and foreign countries, many of which are striving to reduce anthropogenic CO_2 emissions by either voluntary or regulatory means. However, it is clear that much work remains to be done to optimize olivine/serpentine carbonation for future applications in industrial settings. This reality has prompted the writers to submit proposals to potential funders in the U.S. DOE's Office of Fossil Energy outlining follow-on research that will further demonstrate the technical and economic viability of the new multistep method for achieving this carbonation, which has the potential to supplant all other proposed approaches for global-scale CO_2 sequestration by mineral carbonation.

References

[1]K. S. Lackner, C. H. Wendt, D. P. Butt, E. L. Joyce Jr., and D. H. Sharp, "Carbon dioxide disposal in carbonate minerals," *Energy* **20**, 1153 (1995).

[2]P. M. Goldberg, Z.-Y. Chen, W. K. O'Connor, R. P. Walters, and H. Ziock, "CO_2 Mineral Sequestration Studies in US," Paper presented at the First National Conference on Carbon Sequestration, May 14–17, 2001, Washington D.C.

[3]K. S. Lackner, D. P. Butt, and C. H. Wendt, "Magnesite Disposal of Carbon Dioxide," in B. Sakkestad (ed.), *Proceedings of the 22nd International Conference on Coal Utilization and Fuel Systems,* pp. 419–430, Coal and Slurry Technology Association, Washington, D.C., 1997.

[4]F. Goff, G. D. Guthrie, D. A. Counce, E. Kluk, D. Bergfeld, and M. Snow, *Preliminary Investigations on the Carbon Dioxide Sequestering Potential of Ultramafic Rocks*, Los Alamos National Laboratory Report LA-13328-MS, 1997.

[5]F. Goff and K. S. Lackner, "Carbon dioxide sequestering using ultramafic rocks," *Environ. Geosci.* **5**, 89 (1998).

[6]W. K. O'Connor, D. C. Dahlin, D. N. Nilsen, G. E. Rush, R. P. Walters, and P. C. Turner, "Carbon Dioxide Sequestration by Direct Mineral Carbonation: Results from Recent Studies and Current Status," paper presented at the First National Conference on Carbon Sequestration, May 14–17, 2001, Washington, D.C.

[7]G. D. Guthrie, J. W. Carey, D. Bergfeld, D. Byler, S. Chipera, and H. J. Ziock, "Geochemical Aspects of the Carbonation of Magnesium Silicates in an Aqueous Medium," paper presented at the First National Conference on Carbon Sequestration, May 14–17, 2001, Washington D.C.

[8]J. G. Blencoe, L. M. Anovitz, D. A. Palmer, and J. S. Beard, "Carbonation of Metal Silicates for Long-Term CO_2 Sequestration," U.S. patent application filed November 12, 2003.

Online Characterization of Individual Airborne Bacteria

W. B. Whitten[1] and S. Hoffmann[2,*]
[1]*Chemical Sciences Division, ORNL*
[2]*Institute for Spectrochemistry and Applied Spectroscopy, Dortmund, Germany*

An apparatus was developed to decouple the laser desorption and ionization processes in real-time mass spectrometry of individual airborne particles. Experiments were performed to explore atmospheric pressure chemical ionization of laser-desorbed species from airborne particles. An important discovery that we made was that certain biological molecules that were ionized in an atmospheric pressure discharge did not undergo the fragmentation that usually occurs when molecules are ionized in vacuum. Absence of fragmentation leads to much simpler mass spectra that make identification of the particle composition more positive.

Introduction

Timely detection and identification of airborne microorganisms is becoming increasingly important. Traditionally, bioaerosols are collected on culture media and identified by colony growth and response to various agents. There is considerable interest, however, in chemical techniques that would be potentially more rapid and that could also identify nonviable organisms. These techniques fall into two classes—those that use the highly specific attraction of the antibody-antigen reaction or the hybridization of gene probes to DNA or RNA and those based on conventional chemical analysis. The latter methods are usually faster and can respond to a wide range of species, at the expense of specificity. We have been developing an instrument to characterize airborne microparticles in real time by laser ablation mass spectrometry. Previous studies of laser ablation mass spectrometry of airborne particles showed that charge transfer from ions generated in the laser ablation process to neutral species with lower ionization potentials caused the measured mass spectrum to be dominated by the latter species. For the characterization of microorganisms, it would be desirable to detect ions of proteins of other biomarkers of high molecular weight that are specific to a particular organism. The mass spectrum of bacteria that we obtain is predominately from adducts of potassium with small fragments of unknown composition as well as ions of iron and other inorganic substances. We anticipate that performing the ionization after the laser ablation plume has expanded sufficiently to eliminate most ion-neutral collisions will yield a more representative mass spectrum.

*This project was part of the PhD thesis research of Sven Hoffmann who was visiting ORNL from Germany.

Technical Approach

A Varian Saturn II mass ion trap mass spectrometer was modified by the addition of an atmospheric pressure inlet and an ion guide based on two linear electrodynamic quadrupoles operating at approximately 4 MHz and 600 V peak amplitude. A photograph of the atmospheric-pressure inlet system and ion guide housing is shown in Fig. 1. By applying appropriate bias voltages to the quadrupole electrodes and apertures, it was possible to transfer ions entering the inlet to the quadrupole ion trap of the mass spectrometer for mass analysis. The ions were generated by atmospheric pressure chemical ionization in a corona discharge external to the inlet. Other experiments were carried out with a Finnigan LCQ Deca XP Plus mass spectrometer that has an atmospheric-pressure inlet system.

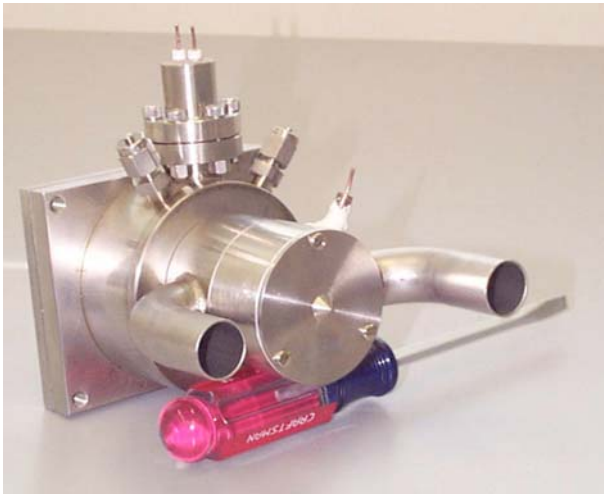

Fig. 1. Photograph of the atmospheric-pressure inlet system and ion guide housing.

Results and Accomplishments

For the first tests, samples were deposited on a metal target placed near the inlet, as shown in Fig. 2. The corona discharge was produced between the needle and the inlet housing. Sample molecules were desorbed from the target by a pulsed Nd:YAG laser and ionized by proton exchange with water ions produced in the discharge. Results with substances such as benzophenone were encouraging. Interesting results were also obtained for samples desorbed from the vicinity of the entrance orifice. However, the sensitivity of the instrument was apparently insufficient to obtain laser desorption mass spectra from airborne particles.

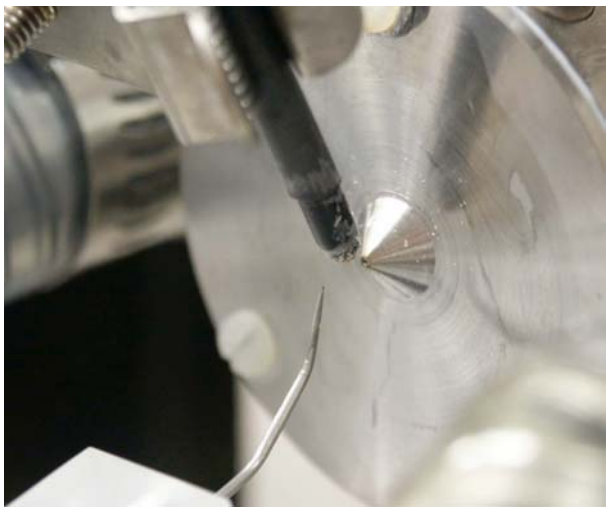

Fig. 2. Setup for preliminary tests.

To test the effects of instrumental sensitivity, the experiments were moved to the Finnigan Deca mass spectrometer. This instrument was designed for atmospheric pressure sampling of a liquid chromatograph effluent and contains a high-efficiency ion guide to direct the externally produced ions into the mass analyzer. A photograph of the experimental arrangement at the entrance of this mass spectrometer is shown in Fig. 3. Some exciting preliminary results were obtained from airborne tryptophan particles in the brief time available with this instrument. The mass spectrum obtained from a single tryptophan particle is shown in Fig. 4. The spectrum is almost entirely due to the protonated parent ion.

Summary and Conclusions

The important result from these studies is that the ionization resulting from the laser desorption atmospheric pressure chemical ionization produced little or no fragmentation of the parent molecule. If this should hold true as we expect for larger biological molecules, the mass spectrum from a complex mixture will be easier to interpret and a larger concentration of parent ions will be available for further characterization by tandem mass spectrometry.

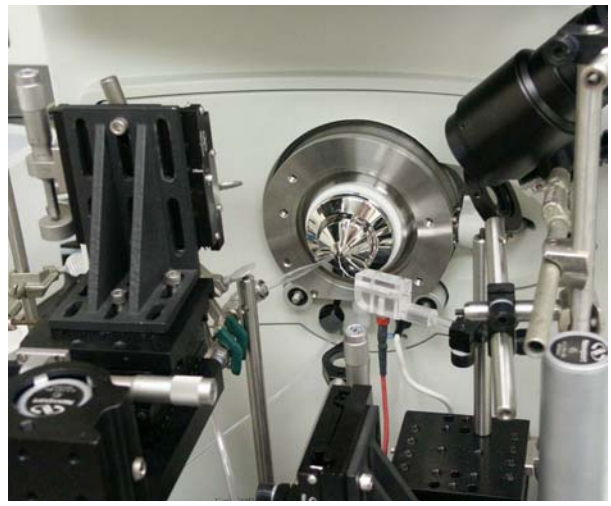

Fig. 3. Experimental arrangement with Finnigan LCQ Deca XP Plus.

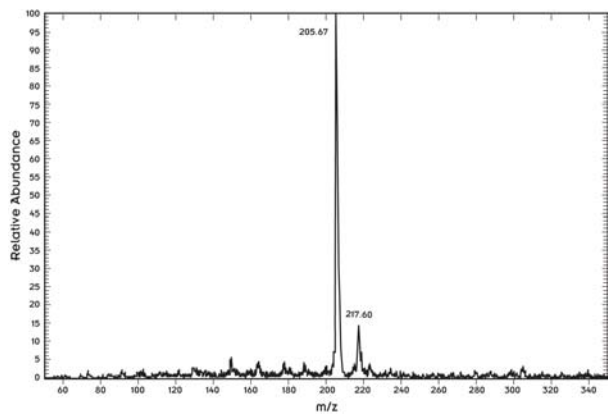

Fig. 4. Mass spectrum from a single tryptophan particle.

While at ORNL, Mr. Hoffmann designed and constructed several pieces of apparatus that will be used by our group in future work. These include an atmospheric pressure inlet for the Saturn mass spectrometer, discharge cell, quadrupole ion guide, and a high-voltage radio-frequency generator to power the guide. A task describing a laser desorption/atmospheric pressure chemical ionization front end for a next-generation biological mass spectrometer was included in a whitepaper submitted in response to a call from the Department of Homeland Security.

Photomolecular Comb

R. J. Warmack,[1] T. G. Thundat,[2] T. L. Ferrell,[2] and G. M. Brown[3]
[1]*Engineering Sciences and Technology Division*
[2]*Life Sciences Division*
[3]*Chemical Sciences Division*

A novel concept was explored that has the potential to accelerate and automate chromatographic analyses using photo-directed accumulation. Photoexcitation of a semiconductor surface in an electrochemical cell produces an electric field that can accumulate charged proteins. Motion of focused light beam can then be used to move the proteins in a directed, channel-less fashion. Molecular motion and chromatographic separation in a buffered gel depends upon the charge of the molecule and its size compared to the gel pores. This exploratory work has been used to demonstrate photo-accumulation, motion, and separation of protein mixtures for the first time. When the method is fully developed, this technology will provide direct control of chromatographic separation, hopefully with higher speed and resolution, which should greatly accelerate proteome analyses.

Introduction

The need for increased efficiency in drug discovery and disease diagnostics has driven a tremendous amount of research aimed at understanding the underlying mechanism of disease. With the sequence of the human genome nearly complete, there has been a significant shift to the post-genome sciences of gene expression and proteomics. Proteome analysis requires fast methods with high separation efficiencies in order to screen the various cell and tissue types for their proteome expression and monitor the effects of environmental conditions and tissue development. While many of the important tools for protein research have been in place for decades, current techniques lack the resolution, integration, and speed of analysis required for current-generation needs. Also, a perpetual problem with chromatographic separation is the need to attach hazardous fluorescent compounds or radionuclides as labels.

The most widely used tool for protein separation, two-dimensional gel electrophoresis, has been available for nearly 30 years. The technique resolves complex mixtures of proteins first by isoelectric point and then by size, generating a gel image pattern, or "fingerprint," of the proteome of a particular biological system. While significant knowledge has been gained with the technique, current systems lack the seamless integration and automation to allow for the reproducible processing of samples on a truly high-throughput basis. Other limitations include low speed, lack of reproducibility, limited range, and the need for attaching labels.

The work described below explores a new basis for chromatographic separations using a swept light beam to both direct the chromatography and monitor its results without using labels. The fundamental concepts are verified, and it is hoped that a fully developed method will provide direct control of chromatographic separation, with higher speed and resolution, as well as provide a built-in electronic readout. Automation, so essential to high-speed screening, is an intrinsic feature of the method.

Technical Approach

The photomolecular comb is a novel technological concept, invented at ORNL, for performing chemical separation and detection of biomolecules such as DNA or proteins using photoelectrochemistry. The idea, shown in Fig. 1, uses a photo-excited semiconductor to induce localized electrophoresis through a medium (buffer solution or gel) in contact with the semiconductor. For example, an electrochemical photo-anodic current using certain photoactive semiconductors causes a positive

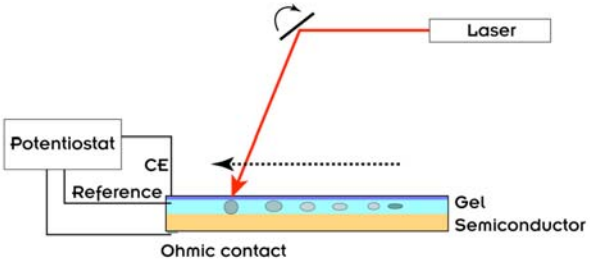

Fig. 1. Molecular comb concept uses a scanned light source to sweep a biosample through a gel to chromatographically separate the components. An electrochemical cell with reference electrode and counter electrode (CE) establishes the proper bias at the semiconductor surface.

charge to develop at the illuminated region. The resulting electric field attracts negatively charged species, such as proteins, and causes them to accumulate at the illuminated spot. An accumulation effect was previously demonstrated for polyanionic DNA using manganese-oxide-coated silicon.[1] Lateral motion of the light spot causes the charged species to be pulled along. When a sieving material such as polyacrylamide is present, chromatographic separation of the biomolecules is possible. In other words, the sieving gel exerts larger forces on high-molecular-weight protein molecules and less so on smaller species. Biomolecules with a low charge or high mass move more slowly and will be left behind if the beam moves with sufficient speed. Consequently, mixtures of biomolecules with different charges and sizes can be separated. This is a unique form of chromatography in which separations can be performed *without* channels or high voltages. In principle, the resolution is limited by the size of the focus so that protein separation can be achieved in a small cell, which could dramatically reduce the analysis time.

Semiconductors such as Si, Ge, GaAs, CdS, and certain metal oxides such as Mn_2O_3, TiO_2, and ZnO exhibit a change in surface charge upon irradiation with light of an appropriate wavelength. Absorption of photons of energies greater than the corresponding semiconductor band gap forms electron-hole pairs. Proper biasing of the solid-liquid interface to create a depletion layer at the surface of the semiconductor results in separation of the charges. The separated charge carriers reach the interface and create a localized photovoltage, whose magnitude is proportional to the light intensity and the extent of the band bending, controlled by adjusting the biasing voltage. The applied potential can be alternated to control the photovoltage, and thus the motion of the biomolecules as well, so that saturation of the biomolecules onto the substrate can be avoided. The illumination duty cycle of the laser can also be modulated to control the motion of the molecules. These experimental conditions can be optimized according to the diffusion and the effective viscosity of the molecules in the medium.

The experimental apparatus consisted of a special electrochemical cell that was open to illumination of a focused laser source. The cell was generally formed of the semiconductor, as the working electrode, upon which was cast agarose or polyacrylamide gel from 20 μm to 2 mm thick. The counter electrode was either a platinum wire loop or plate, or a slide coated with a transparent conducting film of indium-tin-oxide or gold. The buffers were Tris-glycine and others that were adjusted to provide reasonably low conductivity, allowing penetration of the photo-generated electric field across the gel. Ohmic contacts to the semiconductors were provided by epoxy-encapsulated gallium/indium eutectic or annealed aluminum film on the backside. A silver-wire reference electrode was used in some experiments but found to be unnecessary in general. Additionally, a pulsed power supply was designed to allow rapid control of the applied electrochemical bias. A low-power laser (e.g., 633-nm helium-neon, <0.5 mW) was focused onto the sample surface with a specially constructed apparatus designed to scan the laser spot across the working electrode. Two orthogonally arranged galvo mirrors (Model CT-6210, Cambridge Technologies) were interfaced under computer control to provide high-speed control and raster scanning of the light beam.

Results and Accomplishments

A number of experiments were performed using various semiconductors and electrochemical cell arrangements. Using germanium as the semiconductor substrate (working electrode), the photocurrent due to a low-power green or red laser was easily recorded. After depositing an agarose gel and injecting a stained protein, an accumulation was noticed after an exposure of a few minutes under the laser. By slowly moving the laser, the proteins could be moved within this gel. Figure 2 shows a few images of a stained protein (Kaleidoscope™, BioRad Laboratories) being accumulated and moved by two laser

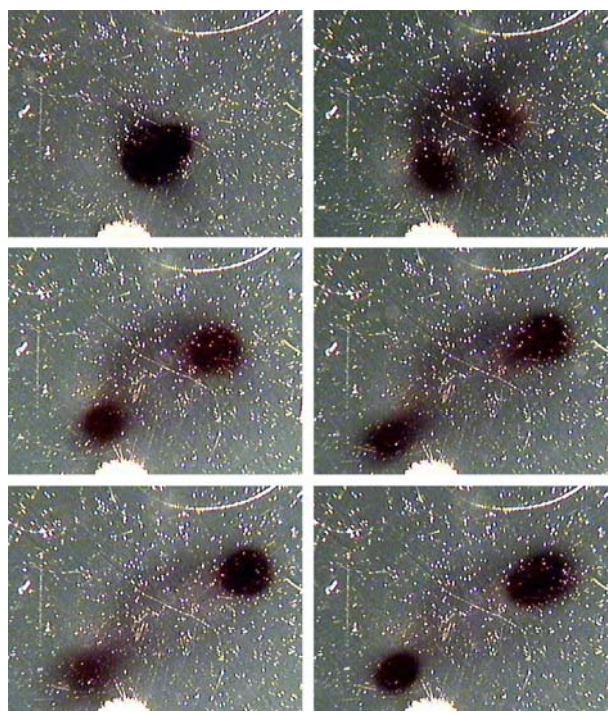

Fig. 2. A series of images of a stained protein (Kaleidoscope™, BioRad Laboratories) being accumulated and moved by two laser spots in an agarose gel located on a germanium working electrode. The light beams were formed by rapidly switching the galvo mirrors and increasing the separation between spots. The spots are moved roughly 5 mm from center to center. The scratches and blemishes in the surface do not affect photo-electrochemical activity.

spots. The size of the spots is roughly 1 mm in diameter and is significantly larger than laser-beam focus due to long charge-carrier diffusion in this single-crystal germanium.

There are a number of challenges that were faced in the electrochemical environment. The electric field depends upon the current density, so that the ensuing photochemical processes can alter the state of the electrodes and the electrolyte. Photocorrosion of the anode as a consequence of water hydrolysis causes oxidation of the surface or bubbles of oxygen to appear. Either effect can disturb the current density. Noble metals,[2] metal oxides,[3] and conducting polymers[4] have also been used to achieve varying levels of stabilization. Additionally, the electrolyte in the vicinity becomes more acidic, lowering the pH, which can alter the charge of proteins, which are amphoteric. In fact, in many cases, fluorescent-stained proteins first accumulate at the illuminated spot but then begin to be repelled as the local pH drops below the isoelectric point of the protein. The electric field is also limited by the conductivity of the electrolyte, so proper buffer preparation was found to be beneficial. Obviously, high contrast in photocurrent between light and dark regions is preferred. A variety of anodic and cathodic materials were tested.

Another goal of the project was to demonstrate the separation of proteins. This was achieved on the basis of charge difference. Figure 3 shows images of two proteins with opposite charge, which can be adjusted under pH control. A plug containing a mixture of the two proteins was located at the bottom of the cell next to the working electrode. The positively charged bovine serum albumin (BSA) is attracted to the photoanode, which repels the negatively charged cytochrome-C.

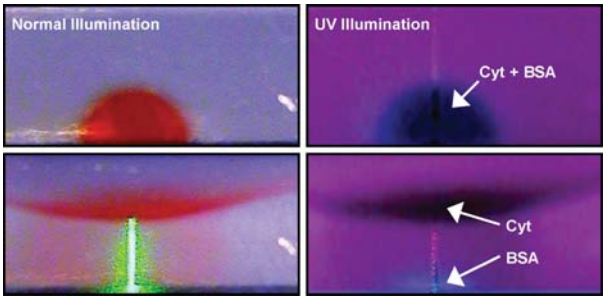

Fig. 3. Images showing the separation of two proteins, cytochrome-C (natural reddish color) and BSA (stained with Marina Blue, Molecular Probes). Top: *Initial cell distribution. The mixture is located near the working electrode.* Bottom: *The cytochrome-C moves to the cathode while the BSA is attracted to the photoanode. Images at the left are under normal illumination, while the images on the right are illuminated under ultraviolet light. The laser light appears as vertical beam. The fluorescent-stained BSA appears as a band near the bottom, while the cytochrome-C appears at the top.*

Summary and Conclusions

The basic premises of the photomolecular comb were established, including the *first known observation of protein photoaccumulation and separation*. When optimally implemented, this concept should have a very significant impact upon diagnostics related to genomics and proteomics. Gel electrophoresis is the mainstay of the burgeoning field of proteomics but is resolution and rate limited. Our work strengthens ORNL's position in biomedical technology and will help us establish long-term research programs with funding from private industry, DOE, and NIH. Already, a funds-in CRADA has been established with Qgenics Biosciences, Inc., which has licensed the intellectual property and is actively and aggressively developing the technology for biomedical diagnostics.

The authors gratefully acknowledge the assistance, advice and encouragement of Qgenics Biosciences personnel, especially Jay Harkins and Chuck Witkowski.

References

[1]I. C. Gurtner, C. Edman, R. Formosa, and M. Heller, "Photoelectrophoretic Transport and Hybridization of DNA Oligonucleotides on Unpatterned Silicon Substrates," *J. Amer. Chem. Soc*. **122**, 8589–94 (2000).

[2]S. Menezes, A. Heller, and B. Miller, "Metal Filmed Semiconductor Photoelectrochemical Cells," *J. Electrochem. Soc.* **127**, 1268–73 (1980).

[3]T. Osaka, K. Ejiri, and N. Hirota, "Photoelectrochemical Behavior of Iron-Oxide N-Si Heterojunction Electrodes with An Outer Pd Layer," *J. Electrochem. Soc.* **131**, 1571–4 (1984).

[4]R. Noufi, A. Frank, and A. Nozik, "Stabilization of N-Type Silicon Photoelectrodes to Surface Oxidation in Aqueous-Electrolyte Solution and Mediation of Oxidation Reaction by Surface-Attached Organic Conducting Polymer," *J. Am. Chem. Soc.* **103**, 1849 (1981).

Protein Surface Mapping by Chemical Oxidation and Mass Spectrometry

R. L. Hettich,[1] J. Sharp,[2] D. Xu,[3] and Y. Xu[3]
[1]*Chemical Sciences Division*
[2]*Graduate Student, ORNL-UTK GST Graduate School*
[3]*Life Sciences Division*

The solvent-accessible surface area of proteins is known to be important in biological function for many reasons, including protein-protein interactions, protein folding, and catalytic function. Because protein surfaces play a vital role in all facets of protein activity, any experimental technique capable of rapidly probing the surface of proteins would greatly assist the investigation of how protein structure is related to function. In this project, we have developed and demonstrated a chemical technique for protein surface mapping based on the oxidation of amino acid side chains in both model proteins such as apomyoglobin, lysozyme, and lactoglobulin, as well as a protein (yeast sml1p) with unknown structure. The elucidation of the effect of solvent accessibility on the sites of oxidation was determined by using both high-resolution electrospray Fourier transform ion cyclotron resonance mass spectrometry (ES-FTICR-MS) and liquid chromatography quadrupole ion trap tandem mass spectrometry (LC-QIT-MS/MS). Mass spectrometry is an ideal tool for analysis of sites of chemical modification due to its high accuracy, sensitivity, ability to be coupled to powerful separations techniques, and fragmentation techniques. Such experimental information can be combined with computational techniques for more comprehensive protein characterization.

Introduction

In modern biology, protein analysis is aided immensely by the determination of the three-dimensional structure of the protein, allowing for rational experimental design to answer specific questions about the function of the protein. Three-dimensional protein structure analysis is often used to study not only the intact structure of a protein, but also its ligand binding sites, protein-protein interactions, and induced conformational changes. Three-dimensional structures are also useful for rational design of enzyme inhibitors, essential in modern drug development. In all fields of biology, protein structure determination always advances the study of any protein to which it is successfully applied, often answering questions that otherwise would require years of tedious research to address.

The central hypothesis of this project is that chemical labeling methods with high-performance mass spectrometric characterization can be used for rapid protein surface mapping by identifying surface accessible amino acids residues in native-folded proteins, and this information can be utilized in an integrated fashion to enhance the accuracy and throughput of computational structural prediction methods. It is the unique combination of radical labeling of native protein structures, high-resolution mass spectrometric characterization, and high-throughput computational structural prediction techniques that provides the power for this approach. If successful, this method could enhance dramatically the ability to characterize the structures (at low resolution) of a wide variety of proteins, providing critical input into the refinement of computational prediction methods.

Technical Approach

The need clearly exists for a high-throughput method for accurate determination of protein structure, preferably based on actual biophysical data. Current structural techniques generally require prior purification of the protein of interest, inherently limiting their speed as well as limiting the range of proteins that can be analyzed to those that can be successfully purified in a native form. It has also been established that computational methods, which are currently the backbone of high-throughput structural analyses, often yield inaccurate structures but can be improved through the use of biophysical constraints.[1–3] The research proposed for this project attempted to address these needs through development of an experimental protocol for protein surface mapping by mass spectrometry.

A viable surface mapping methodology must be based on the specific modification properties, small size, and high hydrophilicity of the reagent species while avoiding the problems resulting from protein cleavage. One promising reagent is the hydroxyl radical, which can modify amino acid side chains via a radical-mediated oxidation. The sites of radical interaction are characterized

at the molecular level by mass spectrometry, a high-sensitivity, high-dynamic range analytical method that can readily handle complex mixtures. The hydroxyl radical appears to meet almost all of the desirable properties of a surface labeling reagent. This radical has been utilized to label a variety of model proteins, and it has been shown that the radical will not interact with side chains that are buried in the native structure, showing that the process itself does not modify the protein topography, and that the presence of the labeling compounds also does not modify the protein topography.[4–5] Moreover, the history of radiation biology provides an excellent collection of data on the reactivity of side chains with hydroxyl radicals.[6]

In this project, we sought to develop and demonstrate the ability to rapidly and accurately probe the surfaces of known as well as uncharacterized proteins in mixtures with hydroxyl radicals. Such an experimental approach could be used to greatly improve the accuracy of structural modeling, with each computational model supported by experimental biophysical data. The longer term goal of this research is to demonstrate how experimental surface mapping and computational prediction can be integrated into an approach that is more powerful than the sum of each technique separately.

Results and Accomplishments

There were three specific focus areas for this project. Each one resulted in a separate manuscript and is summarized below.

1. Fenton Chemistry-Generated Hydroxyl Radical Probes for Surface Mapping of Apomyoglobin

We have developed an experimental protocol to use *chemically* generated hydroxyl radicals to probe the surface areas of proteins by determination of the solvent-accessible amino acids which can be oxidized and then identified by mass spectrometry. This method has rapid reaction times and requires commonly available chemicals. Apomyoglobin was employed as the initial model protein because its secondary and tertiary structure has been extensively characterized by NMR;[7] it is commercially available at high purity, easily digested, and has no prosthetic groups to complicate chemistry or mass spectrometric analysis.

Aqueous buffered solutions of apomyoglobin were oxidized for varying amounts of time using chelated iron and hydrogen peroxide to generate solution-phase hydroxyl radicals, which then react with accessible amino acid side chains to oxidize the protein. Analysis of the oxidation products by high-resolution electrospray Fourier transform mass spectrometry (ES-FTMS) showed that oxidation of apomyoglobin occurs in a time-dependent manner, and several amino acid side chain oxidation events can be detected before significant backbone cleavage occurs. The increase in oxidation events per molecule was clearly time dependent, with cleavage of the protein backbone by the hydroxyl radicals occurring at extended times (several minutes).

In order to determine which amino acid side chains are solvent accessible, we interrogated the sites of oxidation by both ES-FTICR-MS and by reverse phase capillary LC-QIT-MS/MS. The use of high-resolution ES-FTICR-MS allows for high-accuracy mass measurements to ensure the identity of oxidized peptides, while LC-MS/MS is a robust, partially automated method for interrogating the complex mixture to assign oxidation sites. Oxidized peptides identified by their masses were compared to an *in silico* digestion of apomyoglobin. The site of oxidation then was determined by tandem mass spectrometry, looking for a neutral mass loss 16 Da heavier than the expected neutral mass loss. Oxidized peptides containing the two methionines were detected, as well as oxidized peptides containing either Phe151 or Trp7 and Leu11.

Under conditions of low protein oxidation, we have positively identified five oxidation sites by liquid chromatography–tandem mass spectrometry and high-resolution mass spectrometry. With the exception of methionines, all of the residues oxidized and identified in this study are highly solvent accessible according to the NMR structure of apomyoglobin. One interesting note is that this hydroxyl radical attachment technique was able to accurately identify amino acids located in the disordered regions of the apomyoglobin protein (as suggested by NMR measurements). This data provides evidence that the use of chemically generated hydroxyl radicals as probes to determine protein surface residues is feasible, with the exception of methionine oxidation. The short reaction time (30 seconds) along with relatively short digestion and analysis times suggest that this method would be useful as a rapid analysis of certain aspects of protein structure. The results from this proof-of-principle experiment are evidence that selective amino acid side chain oxidation by chemically generated hydroxyl radicals can be used for the rapid analysis of protein solvent accessible surface areas. This work was published in *Analytical Biochemistry* **313**, 216–225 (2003).

2. UV-Radiation-Generated Hydroxyl Radical Probes of Model Proteins

The purpose of this task was to demonstrate how a simple, rapid method for generating hydroxyl radicals from UV-irradiation of hydrogen peroxide solutions avoids the sample cleanup difficulties and high salt concentrations required for the previous approach utilizing Fenton chemistry and generates sufficient hydroxyl radicals to probe the solution-phase structure of two model proteins with well-characterized, stable NMR structural models:

hen egg white lysozyme and bovine β-lactoglobulin A. These two proteins have very different secondary and tertiary structures and serve nicely as test models for quantitating the surface mapping protocol. The rate of oxidation of any one side chain should be influenced by the solvent accessibility of the reactive atoms in the side chain, as well as the inherent chemical reactivity of the side chain. Hydroxyl radicals were generated by UV irradiation of hydrogen peroxide, and the model protein was allowed to react with the hydroxyl radicals. The resulting oxidized protein was analyzed by high-resolution, high-accuracy ES-FTMS to determine the extent of oxidation. The oxidized protein was then digested with trypsin; the resulting peptides were analyzed by LC-MS/MS in order to determine the residues that were oxidized and then analyzed by ES-FTMS in order to both confirm the identity of oxidized peptides and to gather more comprehensive information on oxidized peptides that were not identified by LC-MS/MS. Finally, the sites of oxidation were analyzed against the known solution-phase NMR structures of the model proteins in order to determine the extent to which solvent accessibility influenced the rate of oxidation. A manuscript on this work has been submitted to *Analytical Chemistry* and is in press.

Aqueous lysozyme oxidized for 5 min was denatured and reduced, and then digested with trypsin. The tryptic digest mixture from oxidized lysozyme was loaded onto a C18 column for LC-MS/MS analysis to determine the sites of oxidation. After the LC-MS/MS experiment, the measured peptides were analyzed computationally for differential oxidation of cysteine, tryptophan, methionine, phenylalanine, tyrosine, histidine, proline, leucine, and isoleucine. The non-methionine oxidized residues of lysozyme as detected by LC-MS/MS are shown as colored in Fig. 1. When plotted onto the X-ray crystal structure of lysozyme, PDB accession number 193L, with water removed for clarity,[8] the four oxidized residues can clearly be seen to be on the surface of the protein.

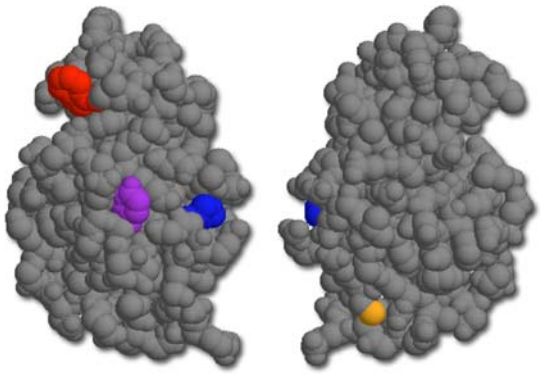

Fig. 1. Two views of the X-ray crystal structure hen egg white lysozyme with waters removed for clarity (PDB accession number 193L). Oxidized residues confirmed by LC-MS/MS are colored, with the sulfur of Cys6 is shown in orange, with the side chain of His15 (blue), Tyr20 (purple), and Trp62 (red) also indicated. Additional oxidized residues were detected by ES-FTMS but are not included here since the exact oxidation sites were not confirmed.

Photochemical oxidation has the advantages of being a simple protocol for labeling of a variety of residues, most of which are normally expected to be buried in protein structures. Since this method probes residues that are expected to be buried in the protein due to their hydrophobicities, even though the degree of surface labeling is limited, the information value of each oxidation event is much greater than if, for instance, the method labeled charged residues such as arginine and lysine that would be expected to be present on the protein surface. The ability of this technique to provide structural data for targeted proteins in a rapid, relatively simple fashion without the necessity for the X-ray synchrotron beamline could be of great use to structural biologists to test structural models or investigate conformational changes.

3. Integrating Experimental Constraints with Computational Structure Prediction for the Yeast DNA Checkpoint Protein Sml1

As the regulator of ribonuclease reductase (Rnr1p), the protein Sml1p is a highly important checkpoint protein, controlling intracellular levels of deoxynucleotide triphosphates and is thus important in maintaining genetic stability.[9] A significant amount of work in multiple labs has been performed in an attempt to elucidate the structure of Sml1p, although to date only limited structural details are known. Previous NMR work performed showed that Sml1p has two alpha helices comprising residues 6–16 and 63–82.[10]

Photochemically generated hydroxyl radicals were used to map solvent exposed regions in the functional as well as denatured form of the C16S mutant of Sml1p from *Saccharomyces cerevisiae*. The data on amino acid solvent accessibilities were then utilized to evaluate pseudo-*ab initio* computational models generated by the Rosetta algorithm, as shown in Figs. 2 and 3. All of the top five models returned by Rosetta disagreed with the solvent accessibility data, as well as with previously published NMR data. A model adjusted using the NMR data as well as tryptophan fluorescence data satisfied most of the solvent accessibility constraints. Through rotation of two amino acid side chains, a model was generated that satisfies previously reported NMR data, fluorescence data, and the solvent accessibility data presented here, as well as possessing a lower free energy than the model constrained solely by NMR and tryptophan fluorescence data. A manuscript on this work has been submitted to the *Journal of Biological Chemistry*.

While the approach taken with the analysis of Sml1p is a valid method for eliminating incorrect structures, better results would be achieved if the constraints were built into the modeling algorithm itself. Current efforts are being made to generate a constraining term for the protein

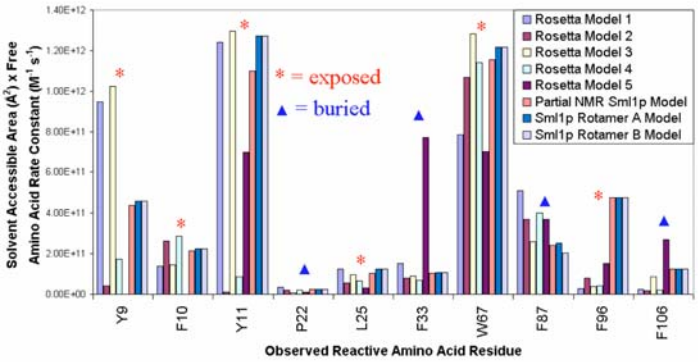

Fig. 2. The product of the solvent-accessible reactive area and the respective free amino acid rate constant for each of the ten reactive, non-methionine residues in C16S Sml1p. Residues that were oxidized in the native state are marked with a red asterisk (exposed), and residues that were oxidized only in the denatured state are marked with a blue triangle (buried).

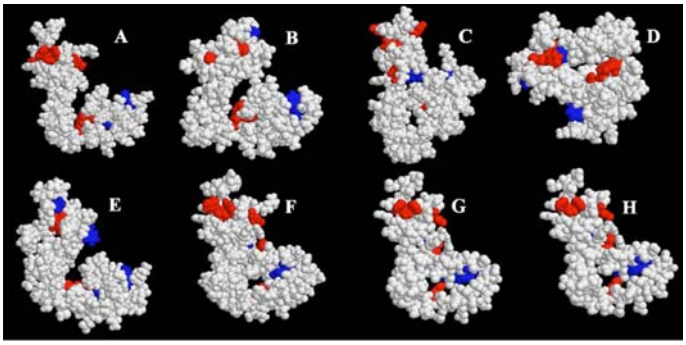

Fig. 3. Spacefill representations of each of the eight computational models discussed. A-Rosetta model 1; B-Rosetta model 2; C-Rosetta model 3; D-Rosetta model 4; E-Rosetta model 5; F-partial NMR Sml1p model; G-Sml1p rotamer A model; H-Sml1p rotamer B model.

threading algorithm PROSPECT, in an attempt to improve threading template selection and energy minimization.[11] Once the solvent accessibility data can be inserted within a threading algorithm, a direct pipeline between surface mapping experiments and constrained computational structures can be established for pseudo–high throughput constrained structure prediction, a tremendous goal for systems biology.

Summary and Conclusions

This project enabled research to demonstrate a viable approach to combine experimental protein structural information (obtained by surface mapping) with computational modeling methods. Although most of the research proposed was directed at demonstration and validation of the protein surface mapping technique with known proteins, the work with the Sml1 protein, whose structure had only previously been partially characterized, should demonstrate how such technology could become very valuable for a wide range of protein structural studies, ranging from bacterial protein characterization to rapid structural interrogation of proteins which have been altered as a function of disease conditions. Such experiments are likely to involve small quantities of proteins in simple or complex mixtures. As such, there presently are virtually no experimental techniques that can even begin to attempt to unravel structural details under these conditions.

One favorable outcome if the proposed experimental approach is successful is the large amount of structural data (albeit low resolution) that can be generated from protein mixtures. Note that such experiments are currently impossible with either x-ray crystallography or nuclear magnetic resonance techniques, which are the primary structural biology tools at present. Such data would be useful to rapidly screen and compare general or targeted proteins in prokaryotic and eukaryotic systems.

References

[1]O. Tcherkasskaya, E. A. Davidson, and V. N. Uversky, "Biophysical Constraints for Protein Structure Prediction," *J Proteome Res* **2**, 37–42 (2003).

[2]P. M. Bowers, C. E. Strauss, and D. Baker, "De Novo Protein Structure Determination Using Sparse NMR Data," *J Biomol NMR* **18**, 311–318 (2000).

[3]Y. Xu, D. Xu, O. H. Crawford, Einstein, F. Larimer, E. Uberbacher, M. A. Unseren, and G. Zhang, "Protein Threading by PROSPECT: a Prediction Experiment in CASP3," *Protein Eng* **12**, 899–907 (1999).

[4]J. G. Kiselar, S. D. Maleknia, M. Sullivan, K. M. Downard, and M. R. Chance, "Hydroxyl radical probe of protein surfaces using synchrotron X-ray radiolysis and mass spectrometry," *Int J Radiat Biol* **78**, 101–114 (2002).

[5]J. S. Sharp, J. M. Becker, and R. L. Hettich, "Protein Surface Mapping by Chemical Oxidation: Structural Analysis by Mass Spectrometry," *Anal Biochem* **313**, 216–225 (2003).

[6]W. M. Garrison, "Reaction-Mechanisms in the Radiolysis of Peptides, Polypeptides, and Proteins," *Chemical Reviews* **87**, 381–398 (1987).

[7]J. T. Lecomte, Y. H. Kao, and M. J. Cocco, "The Native State of Apomyoglobin Described by Proton NMR Spectroscopy: the A-B-G-H Interface of Wild-Type Sperm Whale Apomyoglobin," *Proteins* **25**, 267–85 (1996).

[8]A. C. Young, R. F. Tilton, and J. C. Dewan, *J Mol Biol* **235**, 302–317 (1994).

[9]X. Zhao, E. G. Muller, and R. Rothstein, *Mol Cell* **2**, 329–340 (1998).

[10]X. Zhao, B. Georgieva, A. Chabes, V. Domkin, J. H. Ippel, J. Schleucher, S. Wijmenga, L. Thelander, and R. Rothstein, *Mol Cell Biol* **20**, 9076–9083 (2000).

[11]Y. Xu and D. Xu, "Protein threading using PROSPECT: Design and evaluation," *Proteins* **40**, 343–354 (2000).

Gold Nanocrystal Sensors/Concentrators for Chemical Weapons Agents

T. G. Schaaff
Chemical Sciences Division

The goal of this project was to lay the scientific foundation for developing a program for using gold nanocrystals as selective chemical warfare agent sensors and collectors that are simple and capable of being field deployed with little effort. This proposal was designed to address the scientific proof of principle that gold nanocrystals may constitute a viable sensor and/or concentrator for organosulfur and organophosphorous compounds in civilian and military settings. Gold nanocrystals in various environments were exposed to compounds that are toxic (e.g., pesticides) or simulate chemical warfare agents. Two conditions were tested: (i) changes in optical properties of gold nanocrystal compounds due to exposure of toxic compounds and (ii) collection of toxic compounds by gold nanocrystal compounds. The gold nanocrystal compounds changed color upon exposure to both cyanide and organophosphorous compounds. In addition, it was shown that organophosphorous compounds could be collected and subsequently desorbed and analyzed by mass spectrometry.

Introduction

The ability to detect, concentrate, and identify chemical warfare agents (CWAs) are lacking in both military and civilian settings. Ideal detection systems would accomplish all three tasks, but currently few exist that can readily accomplish more than one task in a given setting and still remain field deployable. In order to accomplish more than one task, detection systems must be designed so that they are both highly sensitive and selective. In addition, the resulting system must be small, rugged, and of simple design, such that it can be deployed in any environmental setting. Ideally, the system would be man-portable. For example, mass spectrometers are highly sensitive and can identify chemical agents readily, but miniaturizing, simplifying, and field-deploying mass spectrometers has proven a daunting task. Simple systems that rely on color changes would ideally suit a battlefield environment.

Of special interest to counterterrorism and military CWA detection are nerve and blister agents. The most widely used nerve agents (e.g., Tabun, Sarin, Soman, GF, VX) are organophosphorous compounds, and blister agents (e.g., Mustards) are typically organosulfur compounds. There is also a need to monitor other environmental toxins, such as pesticides and so-called dual-use compounds (compounds that are used in the production of CWAs). These compounds share the same chemical functionality, typically consisting of organophosphorous and organosulfur (see Fig. 1). Much of the difference lies in the volatility of the organic compounds (e.g., CWAs have appreciable vapor pressure at RT, whereas pesticides are typically nonvolatile) and the reactivity of various leaving groups in the structure. As such, dual-use compounds and pesticides can be used as surrogates or simulants for testing detection systems for CWAs. In addition, the detection of traditional toxins (e.g., cyanide) is of interest to a wide ranging community: from environmental to military.

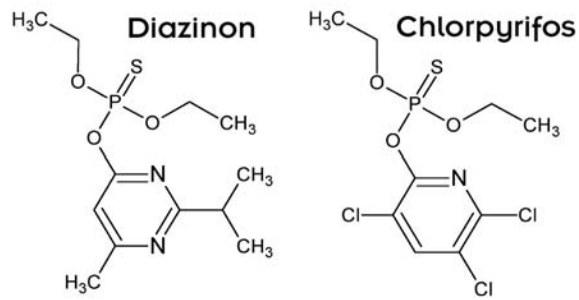

Fig. 1. Surrogates used for these studies.

Gold surfaces are considered "noble" because under most conditions, surface reactions (e.g., oxidation) do not occur readily. However, this classification is not always warranted. There are two classes of compounds for which gold surfaces have extremely high affinity—organophosphorous and organosulfur compounds. Other types of molecules may adsorb (physisorb) to gold surfaces, but with few exceptions, only phosphorous- and sulfur-containing molecules chemically bond to gold surfaces. While these types of molecules bond to gold surfaces, the interaction is still relatively weak, and

chemically bound organophosphorous and organosulfur compounds can be readily removed by gentle heating.[1]

Technical Approach

In many ways, gold nanocrystal compounds possess the same chemical properties of bulk gold but have added features that make them an attractive choice for use in sensors and collectors. In nanocrystalline form, the surface area is enhanced enormously. For example, using crystallographic data obtained on gold:thiolate cluster compounds with 145-atom cores,[2] a 1-cm × 1-cm × 1-µm film of nanocrystals has an equivalent gold surface area of ~1.5 m^2. In addition to the straightforward increase in surface area, nanocrystals have an increase in the number of edge and step atoms, which may also enhance the reactivity of the gold because surface reactions typically occur at faster rates along edge and step atoms. Gold nanocrystal compounds also possess special optical properties, which are inherent to not only the gold core-size, but the type of molecule attached to the surface of the nanocrystal (i.e., the environment of the cluster). The optical properties of gold nanocrystals with thio- and phospho-groups attached to identical gold cores have been studied previously and these show stark differences.[3,4] In addition, the ligands attached to gold nanocrystals can undergo facile exchange in solution with either organophosphorous or organosulfur compounds.[5,6] In these studies, the selective org-P and org-S chemistry of gold is combined with the enhanced surface area (and presumably reactivity) and optical properties inherent to nanocrystal compounds to provide a robust detection and collection technology of sufficient simplicity to be deployed.

This project is designed to provide the proof-of-principle experiments needed to expand programs in chemical warfare agent detection and nonproliferation. Relatively simple experiments will indicate if the gold nanocrystal can be used as a sensor/detector for org-P, org-S, and cyanide by measuring changes in optical properties upon exposure to surrogate molecules under various conditions. The gold nanocrystals will be investigated for detection of various toxins in different environments: (i) toxins in solid form, (ii) toxins in vapor form, and (iii) toxins dissolved in liquid media. To address the collection/concentration and sampling issue, gold nanocrystals will be exposed to CWA surrogates and then surface-bound molecules will be identified by thermal desorption and electron impact mass spectrometry.

Gold nanocrystal compounds with both hydrophilic and hydrophobic ligands were synthesized using established methods. For solution-phase detection and collection/concentration, the nanocrystal compounds were used as obtained from the synthesis. Reactions were performed in solutions native to the nanocrystals (e.g., hydrophilic nanocrystals were exposed to aqueous solutions containing CWA surrogates).

For vapor-phase detection and collection/concentration, it is likely that passivating thiolate molecule will hinder or even prevent the adsorption of other org-P and org-S molecules. For this reason, bare gold nanocrystals are desired in high density in porous material. To achieve such a structure, the gold was supported on titanium dioxide powders. Using methods developed for catalysts by Iwasawa and coworkers, gold glutathione nanocrystal compounds were co-precipitated with TiO_2/$Ti(OH)_4$ nanocrystals. Heating the precipitated powders under air to 400°C causes both dehydration of the TiO_2/$Ti(OH)_4$ crystallites and desorption and/or decomposition of the thiolate ligands attached to the gold nanocrystals. While preparation of these structures for catalytic purposes usually concentrates on the minimum loading possible for catalytic activity, in these studies, the maximum loading was desired so that changes in the optical properties upon exposure to surrogate molecules could be easily determined and the maximum amount of material concentrated on the gold surface. Co-precipitates were generated at different Au-loadings. Upon heating, it was easy to determine if the loading is too high because a color change from orange to red occurs, indicating sintering of the individual nanocrystals to form large colloids.

Results and Accomplishments

Solution-Phase Detection of Toxins

One of the goals of this project was to provide baseline detection limits for detection of various toxins that are found either in a battlefield environment or in the environment due to terrorist activity or other nefarious processes. Initial work concentrated on the detection of three compounds that are either found under these conditions or surrogates of those compounds: cyanide, diazinon, and chlorpyrofos.

In addition to the results for organosulfur and organophosphorous compounds (shown below), the sensitivity for cyanide in solution was found to be comparable to that of existing technologies. Figure 2a shows the change in optical absorption that occurs when solutions of gold nanocrystal compounds are in the presence of potassium cyanide. Spectroscopically, the absorbance in the visible region is depleted and absorbance in the ultraviolet region of the spectrum is enhanced. Visually, the color of the solution changes from orange/brown to colorless. The detection limit for cyanide using gold nanocrystal compounds under these conditions is approximated [see Fig. 2(b)] to be between 10–100 ppb in solution.

Diazinon and chlorpyrofos constitute simulates for nerve agents due to their chemical structures (see Fig. 1).

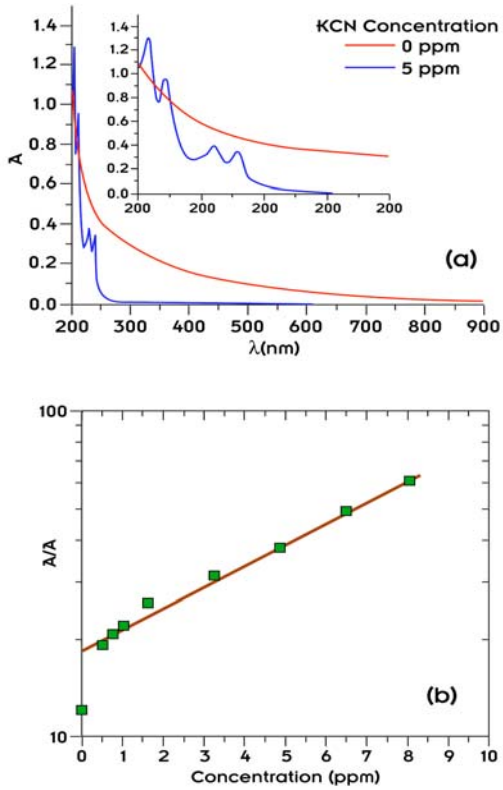

Fig. 2. (a) Optical absorption spectra of gold nanocrystals in water (dotted line) and solution after exposure to 5 ppm CN^- solution (solid line). (b) Ratio of absorbance measurements at 210 nm (UV) and 675 nm (visible) showing the dependence of optical properties on cyanide concentration.

It was found that detection of these types of compounds could not be achieved under strict solution conditions (i.e., using experiments similar to those for detecting cyanide). All solutions tested (formed in polar and nonpolar solvents) retained their visual appearance as well as spectroscopic properties even when these two compounds were added at high concentrations (0.01 M). It is likely the bonding associated with the gold-thiolate nanocrystal compounds is too strong for the displacement of the thiolate ligands by the diazinon or chlorpyrofos molecules, which would be required to measure a change in optical properties.

To overcome this barrier, the gold nanocrystals were deposited on a titanium dioxide support and heated to 250°C, which (i) drives off the existing thiolate ligands and (ii) does not cause an extreme amount of aggregation of the nanocrystals. This was evident from the color of the composite TiO_2/Au films, which retained its characteristic color even after heating. To determine if these molecules could induce a change in optical properties of the composite film, 1–3 µL of diazinon or chlorpyrofos solutions were delivered by a micropipet. Figure 3(a) shows a photograph of a film after delivering 2 µL of 0.001 M diazinon in methanol. The region to the right of the image corresponds to the area where the diazinon solution was delivered. It is clear that the color change occurred only at the region of solution delivery. Blank solutions were also delivered by similar methods, and no color change was measured in the films. Figure 3(b) shows the contrast provided between the area of film not affected by diazinon and the area of the film where the diazinon depleted the color (of the gold nanocrystals).

Vapor Detection/Concentration

A second goal was the concentrating and subsequent detection of organosulfur and organophosphorous compounds by adsorbing these species to gold nanocrystals and using thermal desorption electron impact mass spectrometry. For vapor-phase detection and collection/concentration, it is likely that passivating thiolate molecule will hinder or even prevent the adsorption of other org-P and org-S molecules. For this

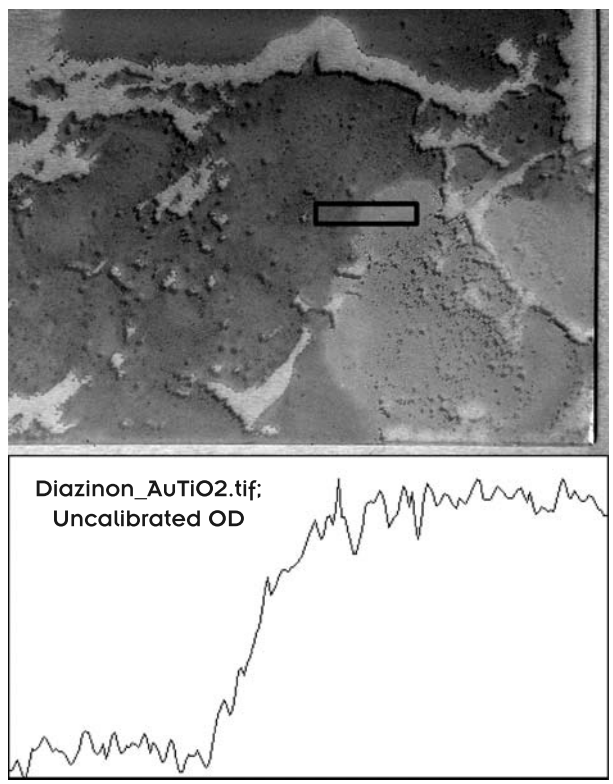

Fig. 3. Photograph of film generated by depositing gold nanocrystals on titanium dioxide and heating for 4 h at 400°C after exposure to 10 µL of 1 ppm diazinon in methylene chloride. The darker area corresponds to the Au/TiO_2 film that was not exposed to diazinon. Note the loss in color of the section of film exposed to diazinon. Total diazinon deposited on film was 12 ng. The optical density plot shows the change in optical density (not calibrated) averaged across the box indicated in the upper image.

reason, the same TiO_2/Au composite films were used for testing the ability to concentrate and detect the presence of toxins in vapors.

After heating the TiO_2/Au composite films on glass coverslips, they were placed into a thin-layer-chromatography developing chamber. Two experiments were performed on these composite films. In the first, one or two drops of volatile toxin was placed into the bottom of the chamber and allowed to evaporate. Thus, a dilute vapor simply reached equilibrium conditions within the chamber and was allowed to passively react with the composite films. Under these conditions, the presence of the toxins (diazinon and chlorpyrofos) was not detected by mass spectrometry.

A second approach was attempted following the inability to detect the molecules under passive conditions. A nebulizer was used to generate a more concentrated vapor form of the two toxins. This was only attempted once because the amount of toxin consumed under this type measurement precluded extensive studies due to cost, cleanup, and waste management considerations. However, under these conditions, the concentrated vapor allowed for detection of the toxins by the TiO_2/Au films. Figure 4 shows the chemical ionization mass spectrum from heating the films to 170°C. The ion corresponding to the $(M+H)^+$ of diazinon is at m/z 305.

Summary and Conclusions

As demonstrated through the detection of the selected toxins under different conditions by these experiments, a gold nanocrystal–based technology holds promise for a field-deployable detection, collection scheme. The goal of these experiments was to provide baseline information regarding the detection limits afforded by this type of technology. In the solution phase, cyanide can be detected at levels comparable to current technology by measuring the changes in optical properties of the nanocrystals. However, other toxins (e.g., other organosulfur and organophosphorous compounds) did not appear to displace the thiols or react in such a way to change the optical properties under solution conditions. Though when the thiols were removed from the nanocrystal cores and composite TiO_2/Au films were generated, the presence of diazinon did cause a change in the optical properties of the composite films. As for the vapor-phase detection, detection limits can only be said to lie between that of the passive vapor and condensation from a saturated vapor. The narrow scope of this proposal (to provide proof of principle for this technology) precludes the ability to make detailed measurements for this system. However, the main goal has been reached for this overarching theme—a simple detection technology that relies on color changes inherent to gold nanocrystals under different conditions.

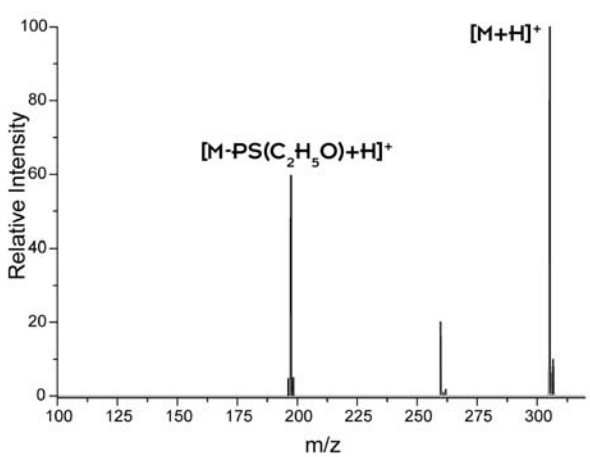

Fig. 4. Chemical ionization mass spectrum from heating the TiO_2/Au composite film to 170°C after exposure to a saturated diazinon vapor. The peak at m/z 305 corresponds to the $(M+H)^+$ ion of diazinon.

Currently, ORNL has elected to pursue a patent on this type of technology for sensing and collecting toxic chemical under typical environment and wartime settings. This technology, if fully developed, would greatly benefit both civilian and military detection schemes for toxins because it inherently targets the most toxic of chemical substances (organophosphorous, organosulfur, and cyanide).

Results from these proof-of-principle experiments indicate that gold nanocrystal compounds may be used in specific settings for the detection or monitoring of toxic chemicals. The detection and monitoring of toxic chemicals is not only of interest to defense-related agencies (e.g., Department of Defense) but is of increasing interest to a number of other agencies mandated to protect the environment and public health and safety (e.g., Environmental Protection Agency, Department of Health and Human Services, and Department of Homeland Security). Collaborating with Thomas Thundat, we plan to incorporate these nanocrystal compounds into cantilever sensor technologies to provide improved detection limits above what is currently capable for cantilever-based sensors. To further this nanocrystal/cantilever technology, we will approach DARPA, DOD, and DHS for follow-on funding, though we anticipate other agencies (e.g., EPA and DHHS) will have requests for proposals in areas where the nanocrystal/cantilever technology will have direct application.

References

[1]R. H. Terrill, T. A. Postlethwaite, C.-H. Chen, C.-D. Poon, A. Terzis, A. Chen, J. E. Hutchison, M. R. Clark, G. Wignall, J. D. Londono, R. Superfine, M. Falvo, Jr., E. T. Samulski, and R. W. Murray, *J. Am. Chem. Soc.* **117**, 12537–12548 (1995).

[2]T. G. Schaaff, M. N. Shafigullin, J. T. Khoury, I. Vezmar, and R. L. Whetten, *J. Phys. Chem. B* **105**, 8785–8796 (2001).

[3]T. G. Schaaff, M. N. Shafigullin, J. T. Khoury, I. Vezmar, R. L. Whetten, W. G. Cullen, P. N. First, C. GutierrezWing, J. Ascensio, and M. J. JoseYacaman, *J. Phys. Chem. B* **101**, 7885–7891 (1997).

[4]E. Gutierrez, R. D. Powell, F. R. Furuya, J. F. Hainfeld, T. G. Schaaff, M. N. Shafigullin, P. W. Stephens, and R. L. Whetten, *Eur. Phys. J. D* **9**, 647–651 (1999).

[5]L. O. Brown and J. E. Hutchison, *J. Am. Chem. Soc.* **119**, 12384–12385 (1997).

[6]M. J. Hostetler, J. E. Wingate, C.-J. Zhong, J. E. Harris, R. W. Vachet, M. R. Clark, J. D. Londono, S. J. Green, J. J. Stokes, G. D. Wignall, G. L. Glish, M. D. Porter, N. D. Evens, and R. W. Murray, *Langmuir* **14**, 17–30 (1998).

Controlling Size and Function of Metal Oxide Nanoparticles: Coupling Micellar Nanoreactor Synthesis and Hydrothermal Processing

D. B. Beach, A. J. Rondinone, P. Benezeth-Gisquet, D. A. Palmer, and D. J. Wesolowski
Chemical Sciences Division

Oxide nanoparticles of well-defined sizes and properties are critical to applications such as nonlinear optics, communications, magnetics, and electronics. This project has produced complex, multicomponent oxide nanoparticles with high degrees of purity, crystallinity, and uniformity of particle size and shape, using a combination of micelle-confined synthesis and hydrothermal post-processing. Hydrothermal processing serves two purposes: it removes organic surfactants and provides a means for crystallization of the oxide nanoparticles without the undesirable agglomeration, growth, and sintering effects of dry-firing.

The predominant hindrance to conducting research and development of oxide nanoparticles is the lack of means through which to crystallize the particles. The properties of oxide materials are highly dependent on crystallinity; without proper crystallinity, the usefulness of oxide nanoparticles cannot be realized. However traditional means of crystallization, such as dry firing, are not available to nanoparticle research because unavoidable aggregation and sintering destroy the nanoparticle morphology. Hence we are attempting to develop a novel method for crystallization that could be a general replacement to dry firing, thereby allowing oxide nanoparticle research and development to move forward.

A small variety of metal oxide nanoparticles have been synthesized using our multistep hydrothermal approach, yielding highly crystalline particles at very small sizes (<10 nm). First, amorphous precursor nanoparticles were synthesized in micellar nanoreactors using sol-gel chemistry. The micellar nanoreactors define and control the nanoparticle size and size distribution. The amorphous particles were then transferred to a hydrothermal autoclave for crystallization. It is important to note that these two steps are discrete and represent a new approach to what has traditionally been attempted as a one-pot process. The technique has been successfully applied to zirconia, titania, and doped and undoped yttrium aluminum oxide nanoparticles.

A large chunk of the project time has been devoted to developing the necessary chemistry to achieve the goal of the project. Removing high-surface-area nanoparticles from a completely hydrophobic environment (micellar nanoreactor), while in the presence of a surfactant, into a completely aqueous environment (for hydrothermal treatment) is not trivial. The nanoparticles must remain completely stable in solution so that irreversible aggregation does not occur. Published chemistry for this step was not available and had to be developed.

While the project has demonstrated feasibility with three nanoparticle oxide systems, focus has been applied to the development of one particularly interesting system, yttrium aluminum oxide. The authors set out to develop a nanoscale version of yttrium aluminum garnet (YAG), a material used in numerous optical applications, but instead have repeatedly synthesized an oxide material with identical stoichiometry whose structure is yet to be determined. The properties of the YAG-like nanoparticle are similar to those of bulk YAG but are different in fundamental ways. For example, the fluorescence lifetime of the nanoparticles doped with fluorescent rare-earth ions is an order of magnitude shorter than the bulk YAG material. Furthermore, the lifetime is temperature dependent at room temperature rather than 500°C as with the bulk. This makes the nanoparticle useful as a remote temperature probe for biological and other systems.

Bulk YAG has a lattice length of 12 Å. These particles have a diameter of 50 Å (see Fig. 1). It is likely that the limit of four or so crystalline units across the diameter of a particle prevents the particle from having the same crystal structure as the bulk material. As the diffraction pattern from these particles cannot be indexed to any known material, it is likely that this is a crystal structure that is not accessible to the bulk material. The goal of synthesizing nanoscale YAG was not achieved; however, a novel material with novel and useful properties was synthesized. Ultimately, novel materials are the goal of nanotechnology research and this project has furthered that goal.

The yttrium aluminum oxide nanoparticles described above may be used as clandestine materials tags for

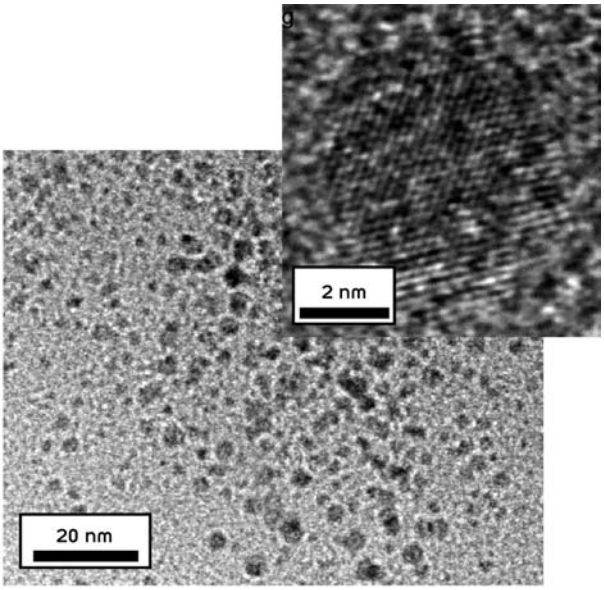

Fig. 1. Cerium-doped yttrium aluminum oxide nanoparticles.

national security and commercial applications. Other oxides such as zirconia are useful as catalysts or catalytic supports. As a result, our synthetic technique as well as the particles themselves have been elected for patent by ORNL.

The authors are also seeking further funding through the offices of the Department of Defense as there are several oxide nanoparticles that the military may find useful. The authors have also proposed to set up a hydrothermal user facility within the upcoming Center for Nanoscale Materials Science.

Metallic Nanofuels for Vehicles

B. G. Sumpter,[1] S. D. Labinov,[2] D. W. Noid,[1] and D. B. Beach[3]
[1]*Computer Science and Mathematics Division*
[2]*Engineering Science and Technology Division*
[3]*Chemical Sciences Division*

This proposal addresses the concept of novel, renewable, high-energy density, non-emission fuels for vehicles based on clusters of metallic nanoparticles and experimental proof of the outstanding characteristics of the combustion these fuels. It is expected that, due to the high surface-to-volume ratio typical of nano particles, complete and fast oxidation (combustion) will take place at temperatures under 1400–1600°C in the condensed phase. This will serve to keep the combustion products on a carrier and avoid pollution of the air by nitrogen oxides. Owing to the exceptionally high energy density, this novel fuel will be very efficient as an energy source for military vehicles, heavy trucks, locomotives, etc. The combustion of fuel clusters and their thermodynamic and thermochemical characteristics will be experimentally explored in order to prove the validity of the proposed concept. ORNL is able to develop this new direction by employing the joint efforts of specialists in chemistry, solid-state physics, energy, transportation, computation, and mathematics.

The problem addressed by this proposal is that of an alternative energy supply system for vehicles that is renewable, nonpolluting, and high in energy density. Limited reserves of liquid fossil fuel, security issues due to foreign oil dependence, and the air pollution caused by the burning of fossil fuels are the major drivers for the search for alternative fuels for transportation. We propose the use of engineered clusters of metallic nano particles as a fuel for vehicles. When compared to conventional liquid fuel, metallic fuel features greater energy capacity per volumetric unit, low flammability, and is virtually explosion proof. (The ignition temperature of bulk material is more than 2000°C in open air.) Its storage does not require any special conditions. Metals useful as fuels and their oxides are not toxic and do not pollute the environment. With the same size fuel tank, a vehicle using iron as a fuel will cover without refueling a distance two times greater than that covered by a car using gasoline. With aluminum or boron as fuels, the distances would be three and five times greater than gasoline! The combustion products of metals are solid oxides that can easily be stored and transported to reduction facilities.

The following problems need to be solved in order to demonstrate the capabilities of a nano fuel–based on metallic clusters: (1) the control of the metallic fuel combustion process; (2) the quick decrease or increase of released heat quantity depending on engine load, and (3) systems providing for fuel delivery to a combustion chamber and ash removal. Our proposed research addresses these problems by using a fuel cluster composed of metallic nano particles, delivered using a thermo-resistant thin-film carrier or through air flow.

In our approach, nano particles will be arranged in fuel clusters. Each cluster includes a number of nano particles that is appropriate for the elementary heat output in a combustion chamber. By arranging clusters on a carrier and activating them as necessary, heat release can be regulated to give the output required by engine loading. Proof-of-concept experiments will be carried out and be considered successful if it allows establishing the following:

1. A fuel cluster consisting of certain number of metallic nano particles and covered with thin metal oxide film can be manufactured with determined configuration and have mechanical strength sufficient to sustain transport and storage.
2. A fuel cluster can be ignited in air under given temperature and pressure with the help of a laser, electrical or electromagnetic short-time pulse, and the energy expenditure to create the pulse is less than 1 % of the energy released by burning the cluster.
3. Metal nano particles composing a cluster are oxidized by the atmosphere oxygen for the time no longer than 10^{-2} sec, with the maximum combustion temperature no higher than 1500°C and without forming volatile components.
4. After a fuel cluster is burnt, it preserves its configuration and strong bond with the carrier (internal combustion versions).

The project has just started (August 2003), but some progress has been achieved. To date, an experimental apparatus for examining the peak combustion temperature of an engineered cluster of metallic iron nano particles has been designed. Following combustion of the cluster (to be performed in FY 2004), the cluster can be removed and examined via microscopy to determine if the combustion caused significant amounts of volatile products instead of occurring mainly in the solid/condensed phase. The approximate fuel cluster size to achieve the necessary heat flow has been computed and a method for experimentally producing such a cluster composed of iron nano particles (the iron nano particles are synthesized using iron carbonyl in a solution of and then compressed into a small cavity followed by heating to produce a cluster with controllable size) has been developed.

The success of this work will lay the foundation for developing the technology for an alternative fuel production and its practical use. It has direct impact on both energy production and environmental quality, two of DOE's main missions. This type of nano fuel will provide an additional fuel source with a high energy density that combusts with near-zero emission. It can be expected that military, space, and specialized vehicles and ships would be the first to make use of such a metallic fuel. (For example, fast burning metal nano particles could be used to boost the output of a fighter plane's afterburner with significant reduction in fuel weight.) Passenger cars, trucks and locomotives converting to metallic fuel will occur gradually.